Effect of Flour Minor Components on Bubble Growth in Bread Dough during Proofing Assessed by Magnetic Resonance Imaging

J. Rouillé,[†,‡] J.-M. Bonny,[§] G. Della Valle,*[,‡] M. F. Devaux,[‡] and J. P. Renou[§]

Moulins Soufflet, BP 12, 10402 Nogent sur Seine, France, INRA—Biopolymers, Interactions, and Assemblages, BP 71267, 44316 Nantes Cedex 3, France, and INRA—Stuctures Tissulaires et Interactions Moléculaires, 63122 Saint-Genes Champanelle, France

Fermentation of dough made from standard flour for French breadmaking was followed by nuclear magnetic resonance imaging at 9.4 T. The growth of bubbles (size > 117 μm) was observed for dough density between 0.8 and 0.22 g cm^{-3}. Cellular structure was assessed by digital image analysis, leading to the definition of fineness and rate of bubble growth. Influence of composition was studied through fractionation by extraction of soluble fractions (6% db), by defatting (<1% db) and by puroindolines (Pin) addition (≤0.1%). Addition of the soluble fraction increased the dough specific volume and bubble growth rate but decreased fineness, whereas defatting and Pin addition only increased fineness. The role of molecular components of each fraction could be related to dough elongational properties. A final comparison with baking results confirmed that the crumb cellular structure was largely defined after fermentation.

KEYWORDS: Dough; fermentation; bubble; magnetic resonance imaging; image analysis; flour minor components

INTRODUCTION

Bread recipes vary among countries but are always based on a mixture of wheat flour with water. Wheat flour presents the ability, when mixed with water, to develop a viscoelastic matrix able to retain gas produced during fermentation (baker's yeast) or beginning of baking (chemical leaveners) (*1*). The final product presents an open gas cell structure, directly responsible for a large number of quality features, i.e., visual and mechanical aspects of crumb. The crumb structure is as important as the crumb appearance and directly influences loaf volume, resilience, and texture in the mouth (*2*). The way the main components influence dough expansion and its rheological properties during fermentation and process to form a cellular structure has been largely studied. Basically, the formation depends on the optimum development of the gluten proteins network into a cohesive dough mass, encapsulating starch granules and other filler materials or components and air nuclei (*3*). Air is an important component, naturally present in the native flour, and it is included during mixing (*4, 5*). Air fraction can represent up to 20% of the dough at the end of mixing (*6*). A simplistic picture of formation of the foam structure (closed gas cells in viscoelastic matrix) is the result of an expansion of air nuclei because of an increase of gas generated by the leavening agent (yeast). However, bubble growth or redistribution includes many other phenomena such as disproportionation and coalescence, which require further insight because they also significantly affect the creation of the cellular structure (*2*).

Studies of dough by microscopy mainly address its structure and gluten network or the way it entraps starch granules but scarcely air bubbles (for instance, see refs *7−9*). Moreover, dynamic observations of dough bubble growth are challenged by the intrinsic practical difficulty to handle a fragile object and visualize expansion. Alternative techniques have been developed for such products such as magnetic resonance imaging (MRI). Widely used for medical diagnosis, this nondestructive technique is able to depict the internal structure of materials, with the image signal being sensitive to both the density and mobility of protons (*10*). Applications of MRI to food science are numerous, mostly based on the characterization of the state of water (*11, 12*), to determine composition, structure, and quality of food (such as fruit, cheese, or oil droplets in emulsion) and assess processing (mass transfer, baking, freezing, and thawing). Recently, Ishida et al. (*13*) showed that MRI was suitable for a 3D analysis of crumb grain structure of baked breads. With a voxel, i.e., volume spatial resolution, of $100 \times 100 \times 100 \, \mu$m^3 and after dough enrichment with paramagnetic reagents, they observed that baked breads made from fresh dough had a more uniform distribution of pores

* To whom correspondence should be addressed. Telephone: 33(0)-240675000. Fax: 33(0)240675167. E-mail: dellaval@nantes.inra.fr.
† Moulins Soufflet.
‡ INRA—Biopolymers, Interactions, and Assemblages.
§ INRA—Stuctures Tissulaires et Interactions Moléculaires.

Flour Minor Components on Bubble Growth in Bread Dough

J. Agric. Food Chem., Vol. 53, No. 10, 2005   **3987**

Table 1. Biochemical Composition of Fractions (g of Component/100 g of Fraction, db)

		starch	proteins	lipids	pentosans	LMW sugars	Pin	ash
CNS	native flour	80	10.5	1.6	1.6	2.6	0.104	0.556
def CNS	defatted flour			0.62				
F1	insoluble fraction	nd[a]	9.9	1.61	1.1	nd	0.079	nd
F2	soluble fraction	nd	19.2	0.48	6.9	17.9	0.044	nd

[a] nd = not determined (data from ref *16*).

than frozen dough. The same group traced the fermentation process of dough using dynamic MRI (*10*), using a decreased spatial resolution ($200 \times 200 \times 1000 \ \mu m^3$) to improve the time resolution (5 min). Assuming that the dough matrix was like gluten fibrils, they related their observations to the effect of mechanical input history on the development of the gluten network. Even if the interpretation of crumb cellular structure differences is not straightforward, this study demonstrates the high potential of MRI for a dynamic follow-up of gas bubbles during fermentation. Takano et al. (*14*) further combined these static and dynamic approaches to assess the quality of breads obtained from frozen dough using freeze-tolerant yeast. Using image analysis techniques for the quantification of MRI results, van Duynhoven et al. (*15*) determined apparent gas cell distribution in dough during proofing and how it was influenced by molding deformation and proofing temperature. These works have underlined the potentiality of these techniques for a better understanding of structural changes occurring during bread-making.

By fractionating and reconstituting flour for French bread-making and using digital image analysis, we recently studied the influence of the soluble fraction, which contain low-molecular-weight (LMW) sugars, soluble proteins (globulins and albumins), and pentosans, on the loaf specific volume and texture fineness, defined as the fraction of gas cells for which the diameter is less than 1 mm (*16*). Puroindoline addition and lipid removal were also tested, because of their effects on bread crumb texture (*9*). For these compositions, the dough rheology has also been studied under large deformation by shear and biextensional tests, which suggested that the soluble fraction played a lubricant role in dough, leading to higher specific loaf volumes and coarser texture (*17*). Meanwhile, puroindolines and lipids were found to not affect significantly dough rheological properties nor loaf volume while modifying texture. Because both baking and proofing can affect the loaf volume and crumb texture, those results show the necessity to improve knowledge on how the texture forms, i.e., how bubbles grow and how coalescence and disproportionation take place during fermentation, a purpose for which MRI seems well-suited.

Therefore, in this work, the effect of dough composition on gas bubble expansion during fermentation was studied by MRI. The experimental procedure has already been built up to offer the best compromise between time and spatial resolutions, and digital image analysis and morphological treatments were adapted to quantify the MRI results (*18*). Similar flour compositions and fractions as those previously studied were used to generate different behaviors and ascertain the role of specific compounds.

MATERIALS AND METHODS

Sample Preparation. The procedure and the basic recipe of dough are part of the procedure for French breadmaking. The flour was a standard commercial mixture from Moulins Soufflet (Nogent, 10-France), named Corde Noire Speciale (CNS). It contained 10.5% proteins (dry basis), 13.8% water (wet basis), and 0.56% ash (db), and

Chopin alveograph measurements gave W and P/L values of 194J and 0.56, respectively. Baker's yeast was freshly compressed *Saccharomyces cerevisae* (33% water, wb) provided by DSM bakery ingredients (Roissy 91, France).

Defatting native flour CNS and water fractionation (based on centrifugation) into soluble and insoluble fractions were carried out according to procedures detailed in ref *16*. Native flour CNS, defatted flour (def CNS), soluble fraction (F2), insoluble fraction (F1), and addition of puroindolines (Pin) to flour, defatted or not (+0.1% on wet flour basis), were used to prepare doughs. Their composition is given in **Table 1**. F1, which represents 94% of dry flour was mainly composed of starch and gluten, whereas the largest part of water-soluble proteins (albumins), pentosans, and LMW sugars was recovered in F2 (6% dry basis).

Before use, exact moisture contents were checked by drying during 2 h at 130 °C. Flour, initial or fractionated (100), distilled water (63% on flour wet basis), salt NaCl (2.2% wb), and yeast (2.5% wb) were mixed to form a dough in a 400 g Chopin alveograph mixer (one rotating paddle). Mixing time was 2 min at 40 rpm followed by 10 min at 80 rpm. Salt was added 5 min before the end of mixing. At the end of mixing, a sample of dough (∼3 g) was immediately but gently put into a lab tub (Ø × L, 15 × 90 mm) and inserted in the NMR probe. Time t_0 necessary between the end of mixing and tub insertion was less than 5 min. Dough expansion because of yeast fermentation during MRI measurements (2 h at 30 °C) was assessed by measuring the mass and initial and final heights of dough in the MRI tub to evaluate the variation of density (g cm^{-3}).

Magnetic Resonance Microimaging. Measurements of images were carried out at 27 °C on an Avance DRX400 microimaging system (Bruker, GmbH, Ettlingen, Germany) with a wide-bore (89 mm) vertical 9.4 T magnet and an actively shielded gradient coil allowing high spatial resolution MRI, according to the procedure detailed in ref *18*. A compromise between spatial resolution (SR) and temporal resolution was defined, with any increase of SR not to be impaired by the blur induced by the motion of dough gas cells during image acquisition. The acquisition time was adjusted to 8 min and 40 s for an image of a single slice positioned 13 mm from the bottom of the lab tub. About 15 images of fermenting dough were obtained. Spin−echo sequence with a nonselective refocusing pulse was chosen for producing images of dough with a reasonable signal-to-noise ratio (∼10). This technique allowed us to compensate local magnetic field perturbations near the interfaces, because of the susceptibility difference between dough water and gas filling the cells. The other acquisition parameters were repetition time (TR) = 500 ms, echo time (TE) = 4.2 ms, field of view (FOV) = 15 × 15 mm^2, and matrix size (MA) = 128 × 64 pixels extrapolated to 128 × 128 pixels. The final spatial resolution was then 117 × 117 × 500 μm^3.

Digital Image Analysis. The digital images were divided into pixels (in our case, 128 × 128 pixels) of which individuals took a value between 0 (black) and 255 (white). Analysis was performed according to the procedure detailed in ref *16* for bread crumb, which was also shown to be well-suited for MRI results obtained for dough fermenting (*18*), and its principle is described below. It relies on the use of mathematical morphology proposed to characterize visual texture in relation to particle size (*19*). The method is based on gray level erosion and dilation and was preferred to the extraction of cells, which required a subjective selection threshold for segmentation. The transformations were applied by moving the structuring element (SE), in our study, a square of size (2n + 1) pixels with a reference pixel at the center, with n being the step of the transformation, varying from 1 to 10.
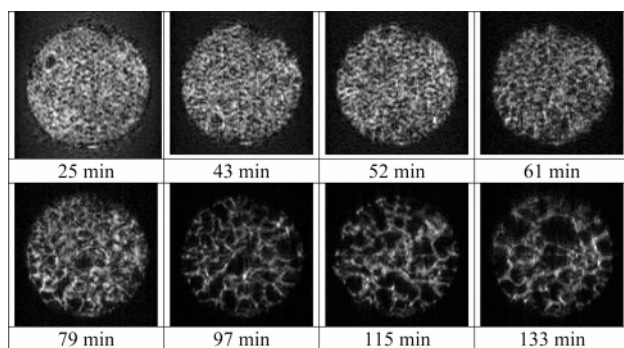
3988 *J. Agric. Food Chem.,* Vol. 53, No. 10, 2005

Rouillé et al.

Figure 1. Dynamic follow up of CNS dough during fermentation. Scale: tub diameter, 1.5 cm; image, 128 × 128 pixels.

In the case of erosion, the reference pixel is given the minimum value met by the SE. The effect is to decrease the size of white objects larger than the size of the square considered and to remove those objects for which at least one dimension is less than $(2n + 1)$ pixels. Erosion makes the sum of the gray level, namely, the volume of the image, decrease. Dilation is the dual operation: white objects are dilated, and dark ones decrease or are removed, according to their size. In this case, the sum of the gray level increases. Successively increasing the size of the SE makes it possible to study the evolution of the sum of the gray level. A curve can be drawn according to the dilation and erosion steps, i.e., the size of the structuring element. By derivation of the variations of the sum of the gray level according to the transformation step, a curve characteristic of the initial image, also named granulometric curve, can be obtained. After normalization according to the initial sum of gray levels, the resulting curve gives information concerning the size distribution of the white and dark objects in the image. In our case, white objects corresponded to the dough matrix walls and dark objects corresponded to the gas cells or bubbles.

Closing treatment consists of combining the two operations; i.e., dilation is immediately followed by an erosion step of the same size. Dark objects smaller than the structuring element are removed, and larger ones keep their size. Applying closings of increasing size acts as an image sieving of dark objects. The increase of image volume measures the gray level fraction of dark objects that have disappeared. Closing curves can be interpreted as particle size distributions, with the size being related to the area of dark objects. An index, called fineness, was defined as the gray level fraction, calculated for step $n = 3$, of dark objects, i.e., gas cells or bubbles, having size <1 mm, and was noted (% d1) (*16*).

Gray levels were first normalized to remove shading over the image. Shading was estimated by applying a dilation of size 10, after a median filtering. The gray levels were set for ranging between 0 and 255 levels, by dividing images by the dilated ones.

Calculation of the sum of gray levels of the image (SGL) was done for each image and was plotted against the transformation step. The decrease of SGL (tend to 0) reflects the apparition and expansion of dark objects, i.e., connex set of dark voxels. After normalization for all doughs, taking the first image as a reference, the variations of SGLcan also be represented as a function of time to reflect the evolution of gas fraction in dough.

Software was developed within the Aphelion V3.1e (ADCIS SA, Herouville 76-France) and Matlab V6.5 (MathWorks, Sevres 92-France) programming environment.

Repetition of the experiments for standard dough (CNS) did not lead to a significant difference between the variations of the image volume.

RESULTS AND DISCUSSION

Follow-Up of Fermentation of CNS Dough. Figure 1 shows the follow-up of fermentation for CNS dough during approximately 2 h at 27 °C. The image signal reveals white to light gray areas (strong signal), indicating the presence of water,

i.e., dough matrix, made of starch granules suspended in a gluten network, whereas dark areas (weak signal) indicate the presence of bubbles of CO_2. The first image of CNS dough, taken at approximately 25 min after the end of mixing shows a very homogeneous dough texture with small gas cells. Although voxel volume ($117 \times 117 \times 500$ μm^3) is not high enough to estimate the size of air nuclei, all dark spots may be assimilated to numerous gas cells. When the size of the image (128×128 pixels) and the tub diameter (15 mm) are taken into account, this observation suggests that the number of bubbles, the size of which is larger than 117 μm, cannot exceed 8×10^7 per unit area (m^{-2}). As shown on **Figure 1**, the sum of gray levels decreases; i.e., gas cell size increases rapidly with fermentation time and becomes really detectable after 52 min. After 1 h, the following images show a dramatic overall increase of dark areas, corresponding to the expansion of gas cells because of CO_2 produced by yeast. During fermentation, air bubbles can be detected for proofing time >1 h. The increase of their size leads to a coarser and less homogeneous cellular distribution than at the beginning. The larger gas cells correspond to former small cells, which expanded by merging with their neighbors, if we assume that no new gas nuclei are generated after mixing and subsequent operations: expansion during fermentation is due to bubble growth, whatever the mechanism, merging or gas production (*3*). At the end of fermentation, after 133 min, cells of size up to 3 mm may be observed, whereas more than 10 cells larger than 1 mm can roughly be counted by unit area (cm^2), i.e., 10^5 m^{-2}. Despite the large area of gas cells, the dough matrix is still continuous, although highly deformed. Overall deformation of cells may be due to reciprocal gas cells stretching as much as the limitation by tub dimensions. Similar to merging phenomenon, bubble deformation depends largely on dough rheological and, more precisely, extensional properties.

Density and Cell Size Changes during Fermentation. After about 15−30 min of proofing, dough density ρ_d, estimated from dough height in the lab tub at t_0, is close to 0.7 ± 0.03 g cm^{-3}, except for F1 (insoluble fraction = starch + gluten), for which the density is 0.84 g cm^{-3}, showing that less air nuclei have been entrapped during mixing or bubbles have grown less in this case (**Table 2**). After fermentation, CNS dough density decreases, by a factor of 2.6, i.e., from 0.68−0.26 g cm^{-3}, according to the variation of dough height in the lab tub at $t_0 +$ 2 h. All doughs undergo a similar density decrease by a factor ranging from 2.6 (CNS) to 3.3 (def CNS + 0.1% Pin). These values underline the ability of dough to retain gas during fermentation.

From the density of gas-free dough, the void volumic fraction ϕ_V is calculated by

$$\phi_V = 1 - \rho_{fd}/\rho_d \qquad (1)$$

When the value 1.22 g cm^{-3} is selected for ρ_{fd}, from a classical additive rule, a void volumic fraction in the range of 0.31−0.46, at time t_0 and in the range of 0.75−0.8 after proofing, are obtained for the doughs of the composition studied here. Just at the beginning of proofing, gas cell size ranges from 10 to 100 μm (*3, 9*), for a void volumic fraction $\phi_V \sim 0.4$, in our case. Surfacic void fraction, i.e., by unit area, can be estimated by

$$\phi_S = 0.8\phi_V^{(2/3)} \qquad (2)$$

using a 2D → 3D conversion procedure suggested by Zghal et al. (*20*).

Flour Minor Components on Bubble Growth in Bread Dough

J. Agric. Food Chem., Vol. 53, No. 10, 2005 **3989**

Table 2. Main Results from Dough and Bread at Three Different Stages of the Process: Beginning of Fermentation (t_0), End of Fermentation (t_0 + 2h), and after the Baking Stage[a]

dough composition	t_0 density (g cm^{-3})	(% d1) (%)	ARBG (10^{-3} min^{-1})	(t_0 + 2 h) density (g cm^{-3})	(% d1) (%)	b η_B (0.1 s^{-1}) (10^3 Pa s)	after baking[a] density (g cm^{-3})	(% d1) (%)
CNS	0.68	51	4.7	0.26	27	32.9	0.24	38
def CNS	0.70	50	4.8	0.27	26	31.8	0.24	53
F1	0.84	49	3.7	0.31	42	162	0.38	58
F1 + F2	0.73	49	4.7	0.24	31	53.1	0.27	41
F1 + 2F2	0.68	46	5.4	0.22	21	30.5	0.22	33
CNS + 0.1% Pin	0.66	50	4.7	0.27	34	32.2	0.28	44
def CNS + 0.1% Pin	0.72		4.4	0.22	37	29.6	0.25	58

[a] Results available from preceding work (*16*). [b] Dough biextensional viscosity data are available from preceding work (*17*).

When this size range and our observations are taken into account and assuming that bubbles have a spherical shape, a value of 50 μm can be selected for the average diameter d_m of bubbles in dough at time t_0. By definition

$$\phi_{cS} = (\pi d_m^2/4)N_{cS} \qquad (3)$$

with N_{cS} being the number of cells by unit area or surfacic gas cell density. Combining eqs 2 and 3 leads to a value of 2.2 × 10^8 m^{-2} for the surfacic gas cell density of dough after mixing. This value is close to the one, 3 × 10^8 m^{-2}, found by Shimiya and Nakamura (*21*), from optical microscopy measurements. Following the same rationale for the end of fermentation with 1 mm as an average value of size cell from MRI observations and a void volumic fraction ϕ_{cV} = 0.8 leads to a surfacic gas cell density value of 9 × 10^5 m^{-2}. This value is about 10 times larger than the rough evaluation made before from MRI images. Although these figures are just rough estimations, this discrepancy questions the hypothesis of sphericity of bubbles that may have deformed under stretching, as suggested by the images. Moreover, it underlines the need of digital image analysis for ascertaining the evaluation of the main features of the cellular structure and not only using MRI as a descriptive tool.

Comparison of Doughs from Different Composition. As expected, density after fermentation was found larger for the dough made with only insoluble fraction, namely, F1. Lower values (0.22) were obtained for doughs to which twice the content of soluble fraction (F2) is added, namely, (F1 + 2F2), and defatted one to which 0.1% Pin is added, noted def CNS + 0.1% Pin (**Table 2**). These results are in agreement with those obtained for baking experiments made with the same compositions (*16*).

MRI observations during fermentation are represented by images at three different times, before gray level normalization, at the beginning and the end of fermentation and also at t_0 + 1 h, to illustrate the changes of the dough cellular structure (**Figure 2**). At t_0, the textures of all doughs are very similar. Texture is very homogeneous with small gas cells, in which the diameter is under image resolution (i.e., <117 μm). After 1 h of fermentation, individual small round gas cells are visible and even large ones (1 mm) in case of (F1 + 2F2) dough. For (def + 0.1% Pin) dough, more cells may be seen than at t_0. After 2 h of fermentation, a difference in textures clearly appears. Gas bubbles are deformed and can hardly be assimilated to spheres. There are rather polyhedral and some discontinuities of the matrix appear, particularly for F1 + 2F2 dough. The trend previously observed for CNS can be extended to the doughs of other composition: the increase of surfacic fraction occupied by dark cells is due to bubble growth by disproportionation and
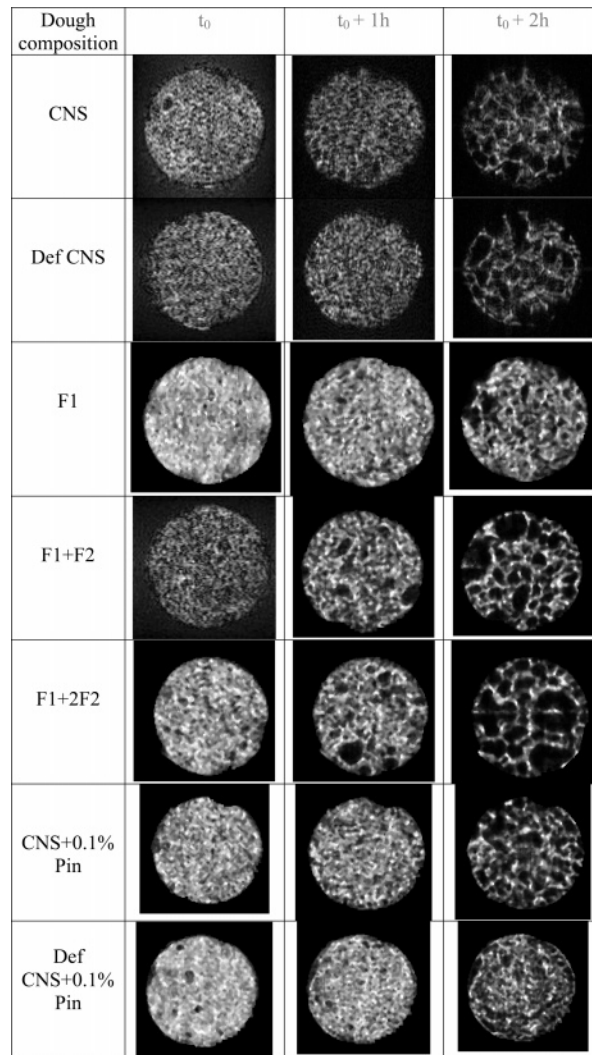

Figure 2. Comparison of dough texture from raw images obtained for different compositions for different times of fermentation (left to right): t_0, t_0 + 1 h, and t_0 + 2 h.

coalescence, both phenomena leading to merging, and internal gas pressure increase because of CO_2 production, rather than the creation of other nuclei (*3*).

Variations of shapes and discontinuity show why cell extraction is not easy for digital image analysis and justifies the use of morphological treatment (erosion/dilation) in this case. Curves obtained by this method are shown in **Figure 3** for the three times (t_0, t_0 + 1 h, and t_0 + 2 h). A general trend of the curves shows an increase of thinner cell walls with time and a concomitant reduction of walls of larger size, because the peak
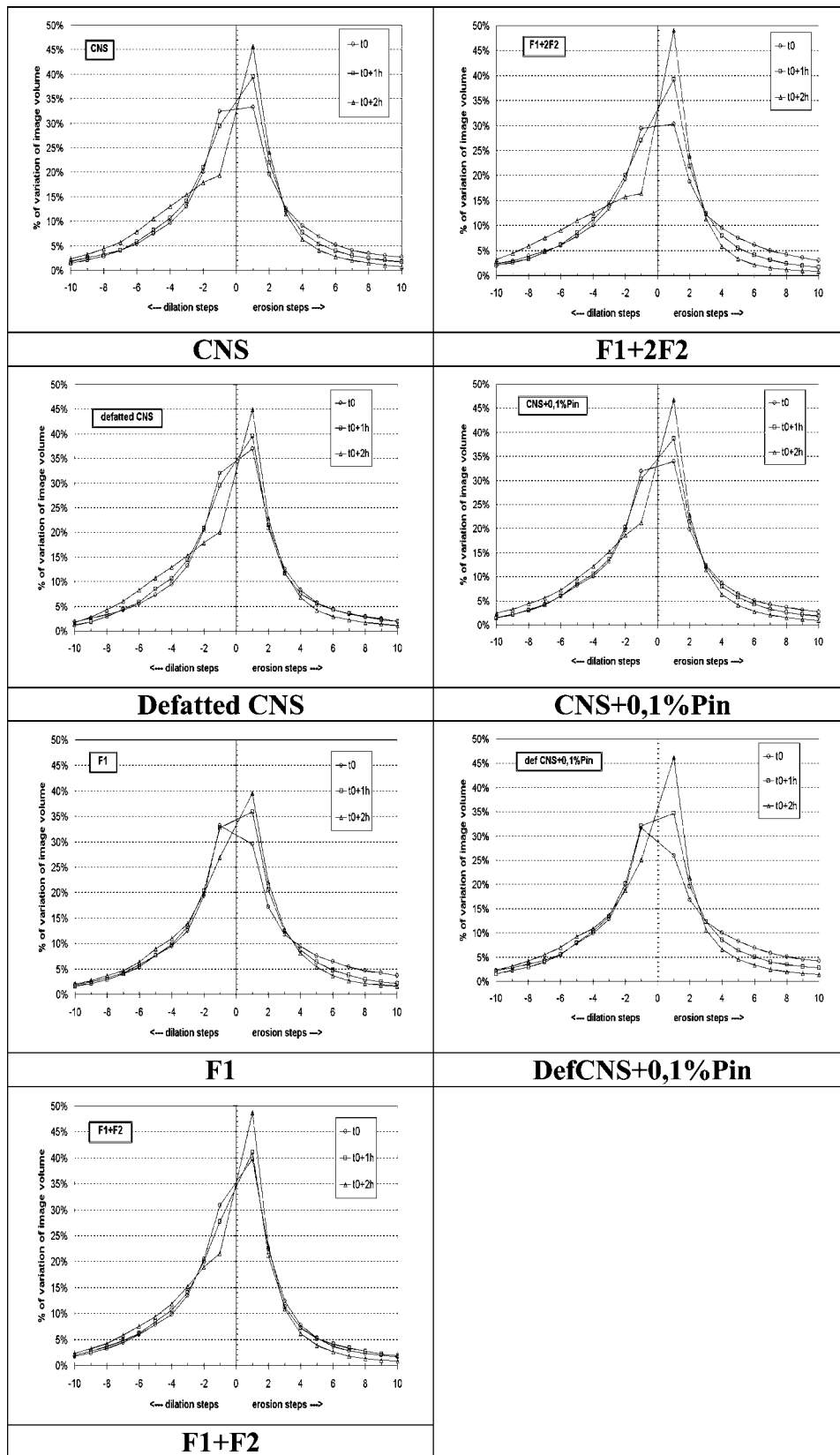
Figure 3. Granulometric curves from erosion (cell walls)/dilation (gas cells) treatment of digital images of different doughs for different fermentation times: (lower to upper peak) t_0, $t_0 + 1$ h, and $t_0 + 2$ h.

becomes narrower on the right part (erosion). In every case, the three curves cross over for erosion steps between 2 and 3, which corresponds to a cell-wall thickness in the range of 580−800 μm. The fraction of cell walls within this interval varies between 10 and 25%. An opposite trend is observed for the

evolution of gas cell size: a smaller cell fraction decreases, and a larger cell fraction increases, as shown by peak spreading on the left part (dilation). The curves cross over around a threshold value of dilation step 3, i.e., size of 820 μm, for 15−20% of cells. When we look more carefully, some differences appear

Flour Minor Components on Bubble Growth in Bread Dough

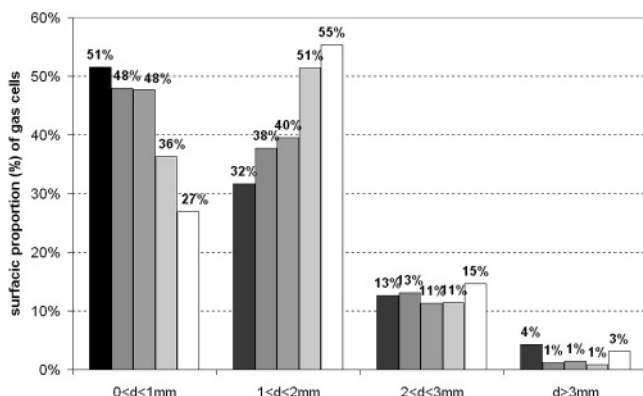*J. Agric. Food Chem.,* Vol. 53, No. 10, 2005 **3991**

Figure 4. Closing treatment on MRI images of fermenting CNS dough: surfacic fraction of gas cells as a function of the cell size for different fermentation times. From black to white filler: t_0, +30 min, +60 min, +90 min, and +120 min.

on these curves and their evolution with fermentation time according to dough composition. The largest decrease of thicker cell walls (>1 mm, $n > 4$) is obtained for (F1 + 2F2) and (def CNS + 0.1% Pin) doughs. The largest increase of cell fraction of larger size (>1 mm, $n > 4$) is obtained for (F1 + 2F2) dough and also initial CNS dough and def CNS to a lesser extent. Although these curves bring information on cell-wall thickness, discrimination between doughs behavior would require further treatment, for instance, by principal component analysis to classify these images, which is not within the scope of the present study.

Conversely, the results of image analysis by closing treatment can be presented as a distribution of surfacic fraction of gas cells as a function of gas cell size (equivalent diameter) and its variations with time, like in **Figure 4** for CNS dough. It shows a continuous redistribution of size cells from the interval [0, 1 mm] to [1, 2 mm]. The ratio of fraction [0, 1 mm] at t_0 to its value at t_0 + 2 h (=$^{51}/_{27}$) is the inverse of the one obtained in the case of fraction [1, 2 mm] (=$^{32}/_{55}$). In the meantime, the fractions for larger size do not change significantly, within absolute experimental error range, i.e., ±5%, and remain close to 13 and 2% for [2, 3 mm] and [3, 15 mm] intervals, respectively. Only dough F1 + 2F2 exhibited a significant change from [0, 1 mm] fraction to fractions of size larger than 2 mm, as suggested before by direct MRI observation in **Figure 2**. Except for this case, all doughs reported a change of the values of fractions [0, 1 mm] and [1, 2 mm] reported for t_0 and t_0 + 2 h (**Table 2**). This is the reason that the fraction of gas cells of size lower than 1 mm is chosen as the texture indicator of fineness, noted (% d1). Moreover, 1 mm is close to the value of the size of the structuring element for step 3, the threshold value observed on erosion/dilation curves (**Figure 3**). The value of (% d1) is close to 0.5 for all doughs at the beginning of proofing, but significant variations are obtained according to dough composition, after 2 h of proofing. Larger (% d1) values, 0.42 and 0.37, i.e., thinner texture, were obtained for F1 and def + 0.1% Pin doughs, respectively, whereas coarser dough texture, i.e., less fine bubbles, is obtained for F1 + 2F2 dough (0.21). These results are qualitatively in agreement with those found by van Duynhoven et al. (*15*), but values found for sizes and fractions cannot be compared straightforwardly because the dough recipe was different.

Image analysis also allows us to calculate SGL after normalization, taking the first image as a reference for all doughs. Its evolution represents the increase of the dark area occupied by gas cells and can be used to evaluate the kinetics
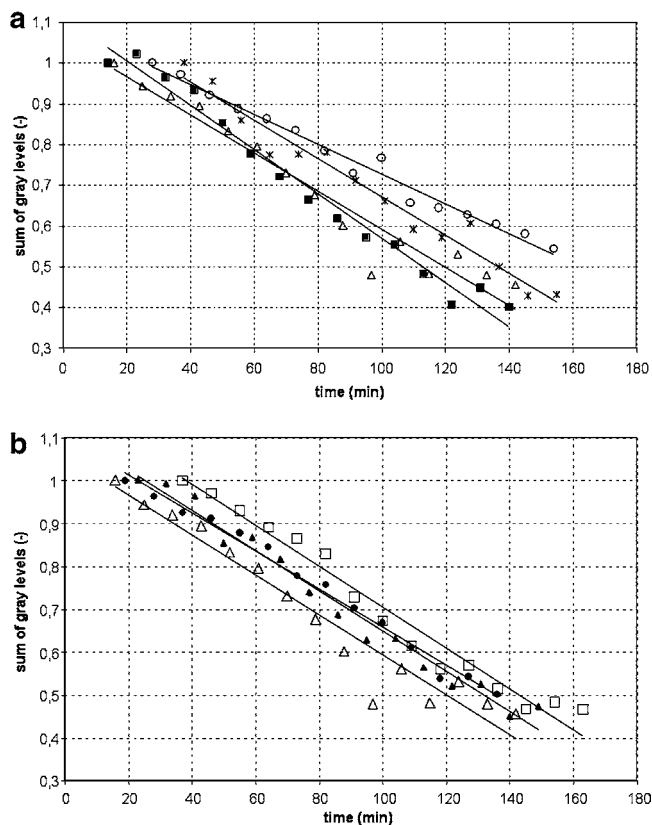

Figure 5. Variation of SGL with the time of doughs of different compositions. Straight lines feature the linear fits ($r^2 > 0.9$). The inverse value of the slopes define ARBG (apparent rate of bubble growth, min^{-1}). (a) CNS ($\triangle$), F1 ($\bigcirc$), F1 + F2 ($\blacksquare$), F1 + 2F2 (*) doughs. (b) CNS ($\triangle$), def CNS ($\square$), CNS + 0.1% Pin ($\blacktriangle$), def CNS + 0.1% Pin ($\bullet$).

of bubble growth in the tub. For all doughs, variations of SGL with proofing time follow a linear trend, and a good fit ($r^2 > 0.9$) is obtained in every case (**Figure 5**). The opposite value of the slope of these straight lines reflect the average rate of bubble growth within dough matrix, noted ARBG, and its values are reported in **Table 2**. In contrast to fineness, a lower value is obtained for F1 (ARBG = 3.7×10^{-3} min^{-1}) and larger value is obtained for F1 + 2F2 (5.4×10^{-3} min^{-1}). These values are of the same order of magnitude as those encountered during fermentation ($\sim 10^{-4}$ s^{-1}) for dough strain rate defined by $1/R$ dR/dt, with R being the average radius of the bubble (*3*).

Relationships with Flour Composition, Dough Rheology, and Breadmaking Performances. Among bread quality criteria, the loaf volume, directly related to density, is the factor most looked for characterization, whereas crumb texture is certainly as significant for the consumer. Crumb fineness (% d1) may assess this criterion, and the images obtained by MRI allow us to measure this variable after fermentation. When comparing density and fineness results obtained after fermentation to those obtained for these variables after baking, taken from a preceding work (*16*) and reported in **Table 2**, only fair correlations ($r^2 = 0.6$) are obtained. **Figure 6** shows that when examining the variations of the loaf fineness (% d1) with % d1 measured at the end of fermentation, the correlation would be considerably improved if data from defatted dough (def CNS) was not taken into account. Although the specific role of lipids is discussed further along, the discrepancies between results obtained after fermentation and after baking might be due to the fact that bubble growth in the MRI tub was likely favored in the axial direction and reduced in the radial one. These
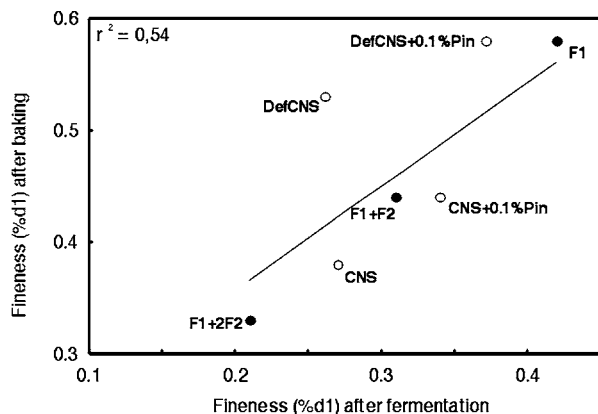
3992 *J. Agric. Food Chem.,* Vol. 53, No. 10, 2005

Rouillé et al.

Figure 6. Fineness (% d1) of dough at the end of fermentation versus fineness (% d1) of the loaf after baking (see values in **Table 2**). The straight line is a linear fit. Closed circles stand for the reconstituted dough from fractions F1 and F2, whereas open circles represent the composition with CNS, defatted or with Pin added.

Figure 7. Variations of fineness (% d1) of dough after fermentation with SHI measured by the biextensional test (symbols are the same as defined in **Figure 6**).

experimental limitations might result in modified bulk density and cellular structure, if compared to dough expanding freely in a proofing oven. Despite these uncertainties, these results suggest that, after mixing, fermentation is the essential step of the baking process for promoting cellular structure of the crumb. This result is in agreement with the conclusion made by van Duyhoven et al. (*15*) stating that "the gas cell distribution of the proofed dough is preserved in the crumb structure of the bread". The major contribution of the baking step, apart from crust creating, which is important chiefly in French breadmaking, would thus be to stabilize and fix this structure, by the dough/crumb transition (*2*). It is all the more significant because, in the latter study (*15*), differences of cellular structure were obtained by changing processing variables, deformation, and proofing temperature, whereas, in our case, only dough composition was changed, while keeping the process unchanged. The knowledge of the behavior of dough during fermentation allows us to improve the link between the composition of flour and its performance in breadmaking.

A considerable effort has been made to build-up relationships between flour composition, mainly proteins content and distribution, and baking quality. These studies have focused on linear viscoelastic properties, to better understand the role of gluten composition, as illustrated by Lee and Mulvaney (*22*). Determination of dough rheological properties in large deformations has been considered as a possible complementary approach (*23*). For doughs from different wheat flour varieties, Sliwinski et al. (*24*) found that the strain-hardening index (SHI), i.e., the extent of stress increase with the strain exerted during uniaxial extension tests, and the elongational flow index were well-correlated to loaf volumes ($r^2 \sim 0.9$), at least for puff pastries. In a recent study (*17*), we found that the dough ability to flow, defined by the inverse of the biextensional viscosity η_B at a given strain rate (0.1 s^{-1} in this case), was correlated to loaf volume, whereas a good correlation was obtained between crumb fineness and SHI, obtained by biextensional measurements. Therefore, it is relevant to examine the influence of these rheological properties on the results of the analysis of dough magnetic resonance images during proofing. Biextensional viscosity was not found to vary much when the lipids/Pin ratio was changed in dough composition from its value in the initial flour, CNS; therefore, only a fair correlation was found when comparing this variable to ARBG. However, **Table 2** shows that values of ARBG decrease when biextensional viscosity
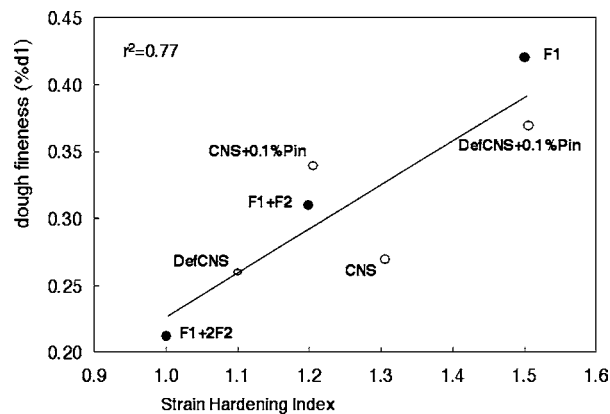
increases, in agreement with the limiting role of the viscosity of the matrix on bubble growth, when superficial tension properties are discarded (for instance, see ref *25*). Conversely, dough fineness (% d1) is well-correlated to SHI ($r^2 = 0.77$, **Figure 7**). This result is in agreement with the suggestion made by van Vliet et al. (*26*) to consider strain hardening as a requirement for gas retention and thus cell stabilization. The correlations found above show that the rheological properties of the dough do not take into account the influence of the minor components on fermentation in the same way and suggest that we discuss them separately.

When soluble fraction (F2) is increased from 0 to 2, ARBG increases by a factor of 1.5 and fineness decreases by 2: the faster the growth of bubbles, the coarser the cellular distribution (**Table 2** and **Figure 7**). These trends confirm the hypotheses suggested for the influence of the soluble fraction. F2 contains LMW sugars (**Table 1**) that increase the capacity of yeast to produce gas and act as a lubricant on the dough matrix made of starch granules suspended in the gluten network: the ability of dough to deform for a given strain rate is increased with increasing soluble fraction content. Conversely, when increasing F2, strain hardening is reduced, allowing the break up of dough cell walls: coalescence takes place and leads to an heterogeneous texture with larger gas cells, in agreement with the mechanism suggested by van Vliet et al. (*26*). Increased production of dissolved CO_2 in dough matrix, when F2 is increased, might also lead to acidification of the medium and decrease of elasticity and viscosity, because of partial degradation of the gluten network, as suggested by Clarke et al. (*27*). However, this hypothesis may be discarded to explain the direct relation of ARBG and % d1 with these properties, when only F2 is modified, because SHI and biextensional viscosity have been measured on unleavened dough, i.e., free of dissolved CO_2 (*17*). The drop of ultrasonic velocity measured during dough fermenting, found by Elmehdi et al. (*28*), could therefore be more because of the expanding gas cells rather than the decrease of dough matrix elasticity. Finally, the influence of LMW sugars would dominate one or the other soluble components, albumins and pentosans, known to contribute to the stabilization of gas cells by their foaming properties (*29*).

Meanwhile, defatting or Pin addition increases fineness after fermentation and SHI, by a factor of 1.5, without significantly changing dough density after fermentation (=0.25 ± 0.2 g cm^{-3}) or the apparent rate of bubble growth, which value remains close to 4.6 × 10^{-3} (±0.2 × 10^{-3}) min^{-1} (**Table 2** and **Figure 7**). The effect of Pin addition on bread texture has already been described by Dubreil et al. (*30*), and it was confirmed by the

Flour Minor Components on Bubble Growth in Bread Dough

J. Agric. Food Chem., Vol. 53, No. 10, 2005 **3993**

results of our preceding work (*16*). Increasing the amount of Pin increases the stability of gas cells and reduces coalescence, which results in an homogeneous texture of the dough with small gas cells; this effect is enhanced when lipids, mainly nonpolar ones, are removed. This effect might be explained by the foaming properties of Pin based on an increase of surface tension of the liquid film of the dough, which separates bubbles (*29*, *31*). The use of confocal scanning laser microscopy (CSLM) has allowed us to localize wheat lipids and Pin in dough, which gives another insight on their functional properties. According to Dubreil et al. (*9*), Pin is mainly located in the matrix, bending with lipids, whereas, using CSLM, Li et al. (*32*) have found that polar lipids are located also around bubbles. In defatted flour, Pin is preferentially located around the gas bubbles, taking the space from where lipids were removed, and increases the surface tension. These preferential locations may explain why, in this case, dough fineness is not directly explained only by extensional properties. These interpretations are based on experimental studies on mixed dough and do not take into account the possible effect of these surface-active components on the very first stage of proofing, including nucleation and Ostwald ripening.

Observation of bubbles at such a scale is an issue for increasing the resolution of magnetic resonance imaging, because this technique has appeared particularly relevant to study the expansion of gas cells in flour dough during proofing. The size of bubbles larger than 120 μm could be determined, which provided an order of magnitude of the density of bubbles (number/unit area) and confirmed those obtained with other microscope techniques. Moreover, main features of dough cellular structure could be evaluated in terms of gas cell size and distribution, using digital image analysis, which underlined the significance of fineness. Overall, kinetics could be assessed by the definition of an apparent rate of bubble growth. The effect of soluble fraction, lipids, and puroindolines on these variables could be determined by the use of fractionated and enriched flour, which confirmed the trends observed after baking. Indeed, wheat flour soluble fraction increases bubble size and growth rate and decreases fineness, with both effects being explained when considering extensional properties of dough. Conversely, lipids and puroindolines did not affect expansion and its rate but modified texture by increasing fineness of the cellular structure, in a complex way that did not imply only bulk rheological properties but also superficial tension, because of the localization and interactions of these components at the dough matrix/bubble interface. These results confirm that texture is governed by dough composition and largely set after fermentation, but the effect of those fractions on structural modifications during baking and mechanical properties (texture) of dough needs further investigation.

ACKNOWLEDGMENT

LITERATURE CITED

(1) He, H.; Hoseney, R. C. A critical look at the electric resistance oven. *Cereal Chem.* **1991**, *68*, 151−155.

(2) Scanlon, M. G.; Zghal, M. C. Bread properties and crumb structure. *Food Res. Int.* **2001**, *34*, 841−864.

(3) Bloksma, A. H. Dough structure, dough rheology, and baking quality. *Cereal Foods World* **1990**, *35*, 237−244.

(4) Shimiya, Y.; Yano, T. Diffusion-controlled shrinkage and growth of an air bubble entrained in water and in wheat flour particles. *Agri. Biol. Chem.* **1987**, *51*, 1935−1940.

(5) Campbell, G. M.; Rielly, C. D.; Fryer, P. J.; Sadd P. A. The measurement of bubble size distributions in an opaque food fluid. *Food Bioprod. Process.* **1991**, *69*, 67−76.

(6) Whitworth, M.; Alava, J. M. The imaging and measurement of bubbles in bread doughs. In *Bubbles in Food* (Campbell, G. M., Webb, C., Pandiell, S. S., Niranjan, K., Eds.) Eagan Press: St Paul, MN, 1999; pp 221−231.

(7) Gan, Z.; Angold, R. E.; Williams, M. R.; Ellis, P. R.; Vaughan, J. G.; Galliard, T. The microstructure and gas retention of bread dough. *J. Cereal Sci.* **1990**, *12*, 15−24.

(8) Amend, T.; Belitz, H. D. Microstructural studies of gluten and a hypothesis on dough formation. *Food Struct.* **1991**, *10*, 277−288.

(9) Dubreil, L.; Biswas, S. C.; Marion, D. Localization of puro-indoline-a and lipids in bread dough using confocal scanning laser microscopy. *J. Agric. Food Chem.* **2002**, *50*, 6078−6085.

(10) Takano, H.; Ishida, N.; Koizumi, M.; Kano, H. Imaging of the fermentation process of bread dough and the grain structure of baked breads by magnetic resonance imaging. *J. Food Sci.* **2002**, *67*, 244−250.

(11) Schmidt, S. J.; Sun, X.; Litchfield, J. B. Applications of magnetic resonance imaging in food science. *Crit. Rev. Food Sci. Nut.* **1996**, *36*, 357−385.

(12) Foucat, L.; Martinie B.; Renou, J.-P. Méthodes de localisation de l'eau. In *L'eau dans les aliments* (Le Meste, M., Lorient, D., Simatos, D., Eds.) Lavoisier TEC&DOC: Paris, France, 2002; pp 619−649.

(13) Ishida, N.; Takano, H.; Naito, S.; Isobe, S.; Uemura, K.; Haishi, T.; Kose, T.; Koizumi, M.; Kano H. Architecture of baked breads depicted by a magnetic resonance imaging. *Magn. Reson. Imaging* **2001**, *19*, 867−874.

(14) Takano, H.; Naito, S.; Ishida, N.; Koizumi, M.; Kano, H. Fermentation process and grain structure of baked breads from frozen dough using freeze-tolerant yeasts. *J. Food Sci.* **2002**, *67*, 2725−2733.

(15) van Duynhoven, J.; van Kempen, G.; van Sluis, R.; Rieger, B.; Weegels, P.; van Vliet, L.; Nicolay, K. Quantitative assessment of gas cell development during the proofing of dough by MRI and image analysis. *Cereal Chem.* **2003**, *80*, 390−395.

(16) Rouille, J.; Della Valle, G.; Devaux, M.-F.; Marion, D.; Dubreil, L. French bread loaf volume variations and digital image analysis of crumb grain changes induced by the minor components of wheat flour. *Cereal Chem.* **2005**, *82*, 20−27.

(17) Rouille, J.; Della Valle, G.; Lefebvre, J.; Sliwinski, E.; van Vliet, T. Shear and extensional properties of bread doughs affected by its minor components. *J. Cereal Sci.* **2005**, in press.

(18) Bonny, J. M.; Rouille, J.; Della Valle, G.; Devaux, M.-F.; Douliez, J.-P.; Renou, J.-P. Dynamic magnetic resonance microscopy of flour dough fermentation. *Magn. Reson. Imaging* **2004**, *22*, 395−401.

(19) Aubert, A.; Jeulin, D. Morphological classification of rough surfaces. *La revue de métallurgie-CIT/Sci. Genie Matériaux* **2000** (*février*), 247−262.

(20) Zghal, M. C.; Scanlon, M. G.; Sapirstein, H. D. Prediction of bread crumb density by digital image analysis. *Cereal Chem.* **1999**, *76*, 734−742.

(21) Shimiya, Y.; Nakamura, K. Changes in size of gas cells in dough and bread during breadmaking and calculation of critical size of gas cells that expand. *J. Texture Stud.* **1997**, *28*, 273−288.

(22) Lee, C. C.; Mulvaney, S. J. Dynamic viscoelastic and tensile properties of gluten and glutenin gels of common wheats of different strength. *J. Agric. Food Chem.* **2003**, *52*, 2317−2327.

(23) Dobraszczyk, B. J.; Morgenstern, M. P. Review: Rheology and the breadmaking process. *J. Cereal Sci.* **2003**, *38*, 229−245.

(24) Sliwinski, E. L.; Kolster, P.; van Vliet, T. On the relationship between large-deformation properties of wheat flour dough and baking quality. *J. Cereal Sci.* **2004**, *39*, 231−245.

(25) Amon, M.; Denson, C. D. A study of the dynamics of the growth of closely spaced spherical bubbles. *Polym. Eng. Sci.* **1984**, *24*, 1026−1034

(26) van Vliet, T.; Janssen, A. M.; Bloksma, A. H.; Walstra, P. Strain hardening of dough as a requirement for gas retention. *J. Texture Stud.* **1992**, *23*, 439−460.

(27) Clark, C. I.; Schober, T. J.; Dockery, P.; O'Sullivan, K.; Rendt, E. K. Wheat sourdough fermentation: Effects of time and acidification on fundamental rheological properties. *Cereal Chem.* **2004**, *81*, 409−417.

(28) Elmehdi, H. M.; Page, J. H.; Scanlon, M. G. Monitoring dough fermentation using acoustic waves. *Trans. IChemE.* **2003**, *81*, part C, 217−223.

(29) Gan, Z.; Ellis, P. R.; Schofield, J. D. Mini review: Gas cell stabilisation and gas retention in wheat bread dough. *J. Cereal Sci.* **1995**, *21*, 215−230.

(30) Dubreil, L.; Meliande, S.; Chiron, H.; Compoint, J.-P.; Quillien, L.; Branlard, G.; Marion, D. Effect of puroindolines on the breadmaking properties of wheat flour. *Cereal Chem.* **1998**, *75*, 222−229.

(31) Dubreil, L.; Compoint, J.-P.; Marion, D. Interactions of puroindolines with wheat flour polar lipids determine their foaming properties. *J. Agric. Food Chem.* **1997**, *45*, 108−116.

(32) Li, W.; Dobraszczyk, B. J.; Wilde, P. J. Surface properties and locations of gluten proteins and lipids revealed using confocal scanning laser microscopy in bread dough. *J. Cereal Sci.* **2004**, *39*, 403−411.